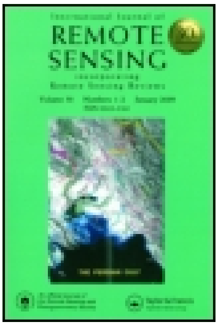

International Journal of Remote Sensing
Publication details, including instructions for authors and subscription information:
http://www.tandfonline.com/loi/tres20

Mixed layer processes of the Arabian Sea Warm Pool during spring intermonsoon: a study based on observational and satellite data

P. Sabu [a] & C. Revichandran [b]

[a] Centre for Marine Living Resources and Ecology, Ministry of Earth Sciences, Kakkanad, Kochi, 682037, India

[b] National Institute of Oceanography, Regional Centre, Kochi, 682018, India

Available online: 11 Aug 2011

International Journal of Remote Sensing
iFirst, 2011, 1–17

Taylor & Francis
Taylor & Francis Group

Mixed layer processes of the Arabian Sea Warm Pool during spring intermonsoon: a study based on observational and satellite data

P. SABU*† and C. REVICHANDRAN‡
†Centre for Marine Living Resources and Ecology,
Ministry of Earth Sciences, Kakkanad, Kochi 682037, India
‡National Institute of Oceanography, Regional Centre, Kochi 682018, India

(*Received 3 February 2009; in final form 3 November 2009*)

The relative importance and contribution of various processes in the total heat budget in the mixed layer of the Arabian Sea Warm Pool (ASWP) during spring intermonsoon (March–April 2004) were studied using *in situ* observations and satellite data. The evolution of the surface heat budget has been resolved into individual components of advection, vertical mixing, eddy induced diffusion and surface heat fluxes. In the northern part of the warm pool, the surface heat flux is the dominant component in the mixed layer warming while the advection plays a role in spreading the warm water from the coastal region to the far west. In the southern part of the warm pool, the eddy induced horizontal mixing provides a substantial amount of heat spreading that influences the mixed layer temperature evolution.

1. Introduction

The seasonal variation in sea surface temperature (SST) in the Indian Ocean is considered an important factor for the onset and subsequent evolution of the Indian summer monsoon (Webster *et al.* 1998). Prior to the onset of the summer monsoon a substantial area of the Indian Ocean has an SST greater than 28°C, known as the Indian Ocean Warm Pool (IOWP) (Joseph 1990, Vinayachandran and Shetye 1991). A major part of the IOWP has an outgoing long wave radiation below 240 W m^{-2} (Lukas 1988) and it is a region of deep convection. The IOWP covers the entire north Indian Ocean (equatorial region east of 50° E, the Bay of Bengal and the eastern part of the Arabian Sea) during May, with peak SSTs above 30°C (Vinayachandran and Shetye 1991). In the southeastern Arabian Sea (SEAS), a core of the warm pool (SST $>$ 30°C) lies in the region of the Lakshadweep Sea during May. This anomalous warm water region in the SEAS is known as the Arabian Sea Warm Pool (ASWP) (Rao and Sivakumar 1999, Anonymous 2001).

It is hypothesized that the high SST in the SEAS from February to March is related to the corresponding high sea level known as the Lakshadweep High (Bruce *et al.* 1994, Shenoi *et al.* 1999). The Lakshadweep High develops mainly due to the downwelling Rossby wave that radiates from the poleward propagating coastal Kelvin wave

*Corresponding author. Email: sabu_sp@yahoo.com

International Journal of Remote Sensing
ISSN 0143-1161 print/ISSN 1366-5901 online © 2011 Taylor & Francis
http://www.tandf.co.uk/journals
DOI: 10.1080/01431161.2010.501350

along the west coast of India (Shanker and Shetye 1997). During winter (November–February), the East India Coastal Current and the Winter Monsoon Current bring cooler, low saline Bay of Bengal water into the SEAS (Cutler and Swallow 1984, Johannessen *et al.* 1987, Shetye *et al.* 1991, Rao *et al.* 1999, Shenoi *et al.* 1999) and lead to the formation of a barrier layer (Lukas and Lindstrom 1991): the layer embedded between the top of the thermocline and the bottom of the surface mixed layer depth. The downwelling Rossby wave and the presence of a barrier layer provide a favourable condition for the peak SSTs in the SEAS (Shenoi *et al.* 2004).

The thermal inversion in the barrier layer initiates mixed layer warming and alters the heat budget of the area by the entrainment of heat from the inversion layer (Thadathil and Gosh 1992, Smyth *et al.* 1996, Masson *et al.* 2002, Durand *et al.* 2004, Gopalakrishna *et al.* 2005, Kurian and Vinayachandran 2006). However, Kurian and Vinayachandran (2007) suggested the role of an orographic effect due to the Western Ghats, which reduces the wind speed over the SEAS, resulting in a positive heat flux into the ocean and an increase in SST in the region.

The heat budget of the mixed layer is an important factor to be investigated to understand the air–sea interaction of the SEAS. Rao and Siva Kumar (1999) opined that the heat build-up in the mixed layer of the SEAS during the pre-monsoon (March–April) is primarily driven by the surface heat flux through the ocean–atmosphere interface. Weller *et al.* (2002) also suggest that the upper ocean processes in the pre-monsoon are primarily one-dimensional (i.e. vertical), where the warming is the result of the surface heat fluxes and the penetrative radiation. Thus, the previous studies in the SEAS during the pre-monsoon period suggested that the heat budget of the upper ocean is mainly a balance between the vertical mixing and the surface heat flux. However, studies have shown that the horizontal processes of the oceans also play an important role in forming the SST anomalies on a seasonal to interannual time scale (Grotzner *et al.* 1998). The intra-seasonal variability in the oceanic and atmospheric parameters affects the heat budget in the upper layers of the SEAS (Murty *et al.* 2006).

The one-dimensional models seldom provide a complete description of the mixed layer processes where variability may be brought by the oceanic advection and sub-grid scale processes (Qiu 2002). The southern part of the SEAS is an eddy prominent region with a horizontal dimension in the range of 200–500 km and a vertical extent of hundreds of metres. These eddies play an important role in the ocean dynamics as well as the transport of heat and other oceanic properties. In an eddy prominent region, the large-scale mass divergence by the mean flow is balanced by the eddy induced divergence, which becomes an essential part of the turbulent cascading (downscaling) of momentum and heat in the upper ocean into sub grid scales (Gent and McWilliams 1990). Thus, eddies in the SEAS have an important role in the evolution of the ASWP, which has not been explored. Thus, in this study, we investigate and identify the relative importance of heat budget components such as surface heat flux, advection, eddy diffusion and vertical mixing on the evolution of the ASWP.

2. Data and methods

The study is based on the data collected during the spring intermonsoon (March–April 2004) cruise of FORV Sagar Sampada as a part of the Marine Research Living Resources (MR-LR) programme along the western shelf of India from 8° N–15° N

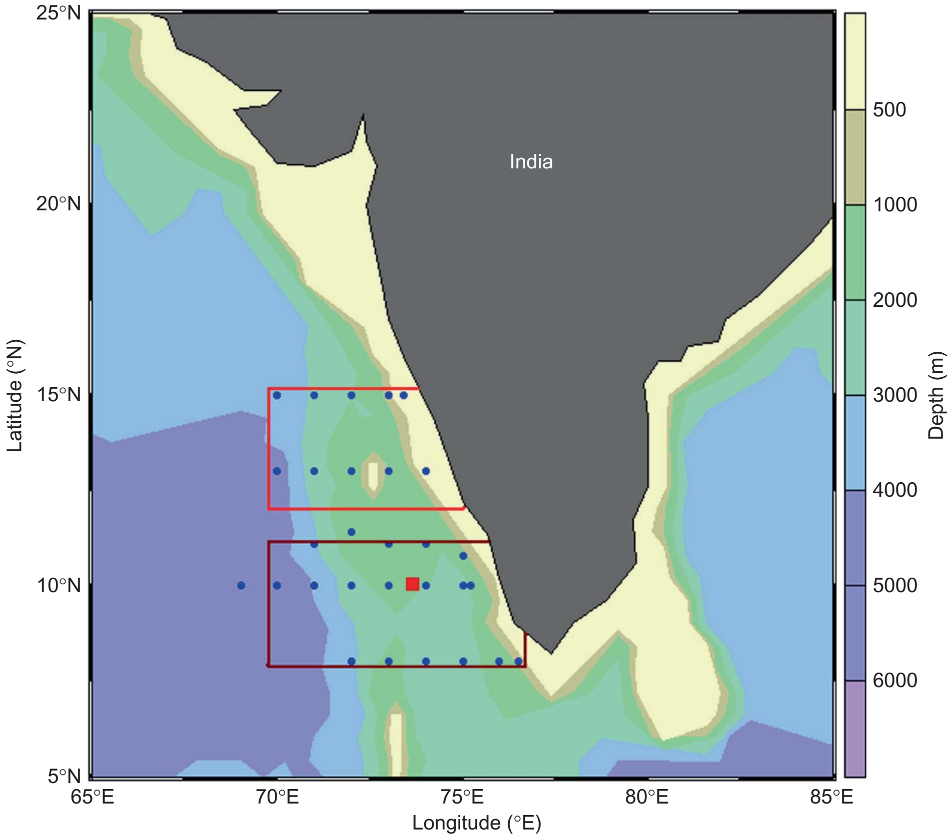

Figure 1. Base map showing the station locations. The cruise started on 19 March 2004 in the south and covered 29 stations (blue dots on the base map represent the stations) and ended on 8 April 2004.

during March–April 2004 (figure 1). A 911*plus* CTD (Conductivity–Temperature–Depth; Sea-Bird Electronics, Inc., Bellevue, WA, USA) was used to collect the temperature and salinity. CTD salinities were calibrated against the values obtained from the Guildline 8400 (model 8400A) Autosal onboard. The SST was measured using a bucket thermometer. The data were re-gridded into a 1° × 1° grid (7° N–16° N and 68° E–77° E) using the linear interpolation method. Horizontal advection due to the pressure gradient was estimated using the geostrophic method (Pond and Pickard 1983). For this computation, 1000 db was considered as the reference level.

The mixed layer temperature tendency of the upper ocean is controlled by the surface heat fluxes, horizontal advection, eddy diffusion, vertical mixing and entrainment (Curry and Webster 1998). The evolution of the mixed layer temperature (T) can be written as

$$\frac{\partial T}{\partial t}+\left[(u_{\mathrm{g}}+u_{\mathrm{e}})\frac{\partial T}{\partial x}+(v_{\mathrm{g}}+v_{\mathrm{e}})\frac{\partial T}{\partial y}\right]+w\frac{\partial \mathrm{T}}{\partial z}$$
$$=\left[\frac{Q}{h}\;\rho C_{\mathrm{p}}\right]+\frac{\partial}{\partial z}\left(K_{\mathrm{h}}\frac{\partial T}{\partial z}\right)+\left[A_{\mathrm{h}}\left(\frac{\partial^2 T}{\partial x^2}+\frac{\partial^2 T}{\partial y^2}\right)\right] \qquad (1)$$

where $\partial T/\partial t$ is the mixed layer temperature tendency, $[(u_g+u_e)\ \partial T/\partial x+(v_g+v_e)\ \partial T/\partial y]$ is the horizontal advection, including the geostrophic (u_g, v_g) and Ekman (u_e, v_e) components (Pond and Pickard 1983), $w\ \partial T/\partial z$ is the entrainment term, where w is the entrainment velocity and $Q/h\ \ \rho C_p$ is the surface flux, where Q is the net radiation, which includes the short wave and long wave radiation, latent and sensible heat fluxes, ρ is the reference density of seawater (taken as 1025 kg m^{-3}), h is the mixed layer depth and C_p is the specific heat of seawater per unit volume (4300 J kg^{-1} k^{-1}) at constant pressure (Liu *et al.* 2005).

The surface meteorological parameters (wind speed and direction, humidity, dry and wet bulb temperatures and atmospheric pressure) were measured from all stations along the ship track using the shipboard automatic weather station. These collected data are used for the computation of long wave radiation, latent heat flux (LHF) and sensible heat flux (SHF) using a bulk formula for humidity and heat exchange:

$$\mathrm{LHF} = \rho C_d L_v U\ (q_s - q_a) \tag{2}$$

$$\mathrm{SHF} = \rho C_d C_P U\ (T_s - T_a) \tag{3}$$

where ρ is the density of air, C_d is the drag coefficient, L_v is the latent heat of vaporization, U is the wind speed, q_s is the saturation specific humidity and q_a is the humidity. q_s is calculated using the Clausius–Clapeyron equation. The C_P is the specific heat capacity of air per unit volume, T_s is the SST and T_a is the air temperature above the sea surface (PrasannaKumar and Prasad 1996, Stewart 2007). Shortwave radiation used in this study is from Southampton Oceanographic Data Centre (SOC)-flux climatology data (Josey *et al.* 1999), which provides the data on a 1°× 1° spatial grid.

The term $A_h\ (\partial^2 T/\partial x^2+\partial^2 T/\partial y^2)$ is the eddy induced diffusion. The K_h and A_h are the vertical and horizontal eddy diffusion coefficients in the mixed layer. The eddy induced diffusion is due to the turbulent transport of heat, which can be written in the turbulent form as $u'\partial T'/\partial x+v'\partial T'/\partial y$ (Pond and Pickard 1983). In order to find the turbulent velocity field in the surface layer (u' and v'), we have used the satellite altimetry measurements from the TOPEX/POSEIDON altimetry data (Sea Surface Height Anomaly (SSHA) data). The SSHA is the deviation from the mean geopotential height (dynamic height) and thus assumes the removal of the mean flow associated with the mean dynamic topography. Thus the remaining component is taken as the fluctuation of the mean flow primarily driven by eddies and thus it provides u' and v' through the geostrophic relation as

$$u' = -g/f\ \ (\partial(\mathrm{SSHA})/\partial y) \tag{4}$$

$$v' = g/f\ \ (\partial(\mathrm{SSHA})/\partial x) \tag{5}$$

where f is the local Coriolis parameter due to the rotation of the Earth and g is the acceleration due to gravity (Stewart 2007). This assumption is valid only near the surface, and not depths at where baroclinic currents take over. The density derived mean geostrophic currents showed that there is no reversal of current direction occurring above 80 m. Thus, the eddy induced surface current is well represented throughout the mixed layer since the mixed layer never exceeded 80 m.

The TOPEX/POSEIDON SSHA data have a seven-day temporal resolution, a $1/3^\circ \times 1/3^\circ$ spatial resolution and cover the entire study region. The fluctuation of temperature (T') was calculated by removing the monthly mean temperature data derived from the World Ocean Atlas 2001 (WOA01) from the observed temperature. The eddy induced diffusion was computed from u', v' and T' (Qiu and Chen 2004).

We have used the K-profile parameterization (KPP hereafter) as in Large *et al.* (1994) to find the vertical mixing coefficients (K_h) from the observed currents and density of the mixed layer. The vertical resolution for KPP is 1 m from the surface to the bottom of the mixed layer. The KPP was performed within this mixed layer to find the vertical mixing coefficient (K_h) according to the observed currents and density of the mixed layer.

The mixed layer tendency term $\partial T/\partial t$ is computed from the satellite derived SST, rather than from our observation for the tendency term calculation because the ship track covered each observational location only once in one cruise, thus losing a finer temporal resolution of temperature changes at any grid location. Although the SST is not the exact representation of mixed layer temperature, it is assumed that the temporal variation in the mixed layer temperature is represented in the SST changes as well. We have taken the TRMM Microwave Imager (TMI) SST on a $0.25^\circ \times 0.25^\circ$ grid to obtain a time series at any location. The satellite data were derived in the region 7° N–16° N and 69° E–77° E and for the period from 20 March to 10 April 2004 (same as our period of observations). Linear interpolation is carried out to avoid the data gaps at certain locations. Thus we have computed the tendency of the SST at our locations from previous and future TMI SST data on a two-day time interval. For example, the tendency of temperature on 23 March 2004 is taken as

$$\frac{\partial T}{\partial t} = \frac{[(\mathrm{TMI})_{24-03-04} - (\mathrm{TMI})_{22-03-04}]}{(\text{two days})} \tag{6}$$

The advection components are calculated by the centred finite difference scheme. The finite centred differences for the individual terms in the advective formulation are $u\,\partial T/\partial x \sim u\,\Delta T/\Delta x$ and $v\,\partial T/\partial y \sim u\,\Delta T/\Delta y$ (Wang and Weisberg 2001). A boundary value is provided from the observations at the domain edges of the study area. It should be noted that the observations on the individual grid faces are done on separate days and thus the advection and diffusion component does not represent the value for a particular time. The effects of tidal processes on the heat budget terms analysed here cannot be explicitly resolved in the given set of data. However, considering our objectives to look at the spatial pattern of heat budget terms on the evolution stage of the ASWP, the effect of tides is safely disregarded.

3. Results and discussion

The meteorological conditions that prevailed in the SEAS (clear sky, high solar radiation and weak northerly winds (average 4.2 m s^{-1})) during the observation time showed typical conditions of spring intermonsoon. Spring intermonsoon in the Arabian Sea is normally observed by light winds, clear skies and strong solar radiation with an average heat gain of 101.1 W m^{-2} (Wiggert *et al.* 2005). The high solar insolation and relatively weaker winds during this time may enhance the surface temperature of the ASWP (figure 2(*a*) and (*b*)). Figure 3(*a*) shows the distribution of observed SST. The warmer regions are close to the coast with a SST of 30.1°C and the isotherms are

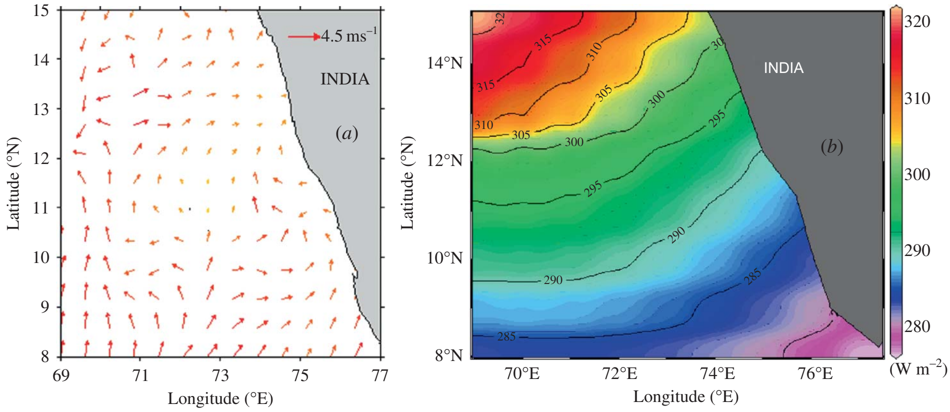

Figure 2. Horizontal distribution of (*a*) surface winds and (*b*) insolation (W m^{-2}) in the study region during the observation period (March–April).

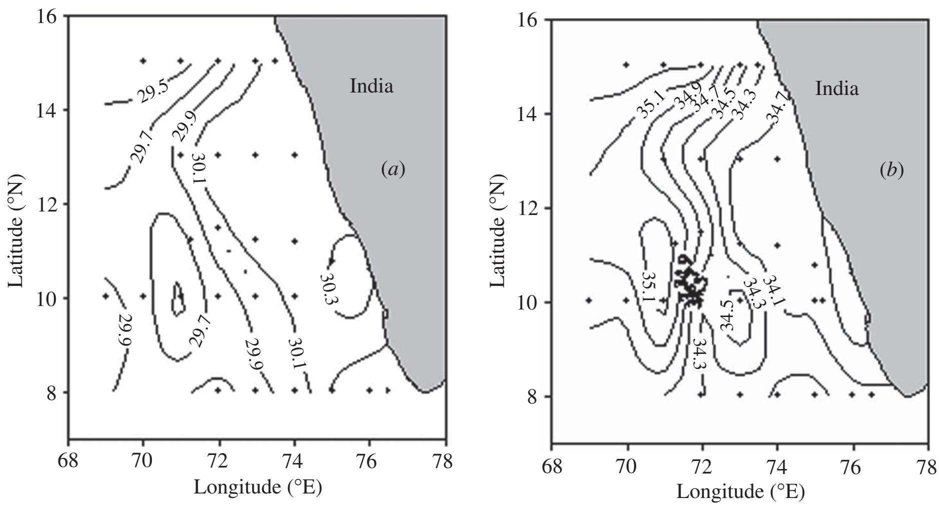

Figure 3. Horizontal distribution of (*a*) temperature and (*b*) salinity (in PSU).

almost parallel to the coast. In this study, we considered the region above 29.5 °C as the ASWP.

Salinity structure showed that a low saline water (<34.2) occupied between 8° N and 13° N in the upper few metres and tapered towards the north. This low saline plume was confined to the shelf region with a minimum value of 33.9 at 10° N (figure 3(*b*)). The isohalines are almost aligned in a similar pattern to that of the isotherms. The vertical structure of isotherms and isohalines along 8° N and 10° N showed an upwards shift (figure 4(*a*) and (*d*)). This upwards shift in isotherms and isohalines was due to the presence of eddies as identified from the SSHA pattern (figure 5). The low saline water mass in the SEAS is due to the intrusion of Bay of Bengal Water (BBW) by the combined effect of the East India Coastal Current (EICC) and the winter monsoon current (WMC) (Shetye *et al.* 1996, Shankar *et al.* 2004). In the subsurface, the presence of a high saline core (>35.6) is the presence of Arabian Sea High Salinity Water

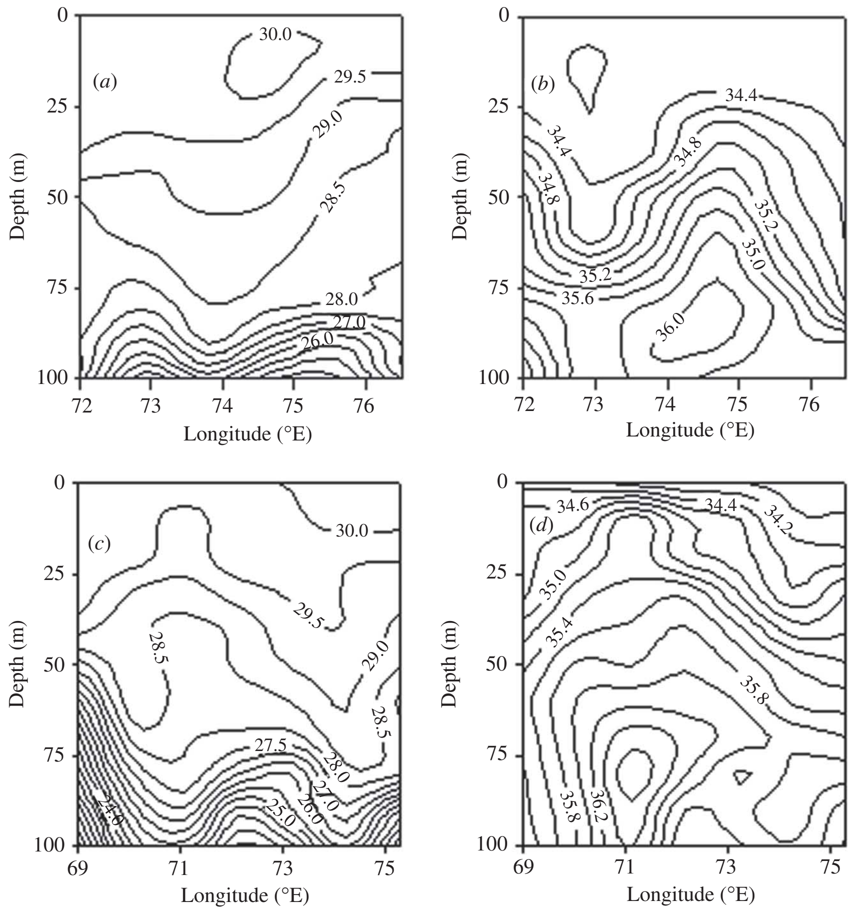

Figure 4. Vertical distribution (*a*) temperature (°C) along 8° N and (*b*) salinity (in PSU) along 8° N and (*c*) temperature along 10° N and (*d*) salinity (in PSU) along 10° N.

(ASHSW) subducted from the northern part of the Arabian Sea and advected towards the south along the main thermocline (Prasad and Ikeda 2002).

We analysed each term of the temperature evolution equation for the entire mixed layer depth (MLD). The MLD is defined as the depth at which the surface density (σ_θ) increases by 0.2 units from the surface value (Shetye *et al.* 1996, Madhupratap *et al.* 2003), which yields an average MLD of 25 m (figure 6). A deeper MLD (>30 m) is observed in the south than the north. A shallow MLD of less than 20 m is found in the southern tip of the peninsula.

4. Heat budget in the mixed layer

In this section, the heat budget of the mixed layer is described as resolved from our analysis. All terms are expressed as depth integrals over the mixed layer depth, unless specified otherwise.

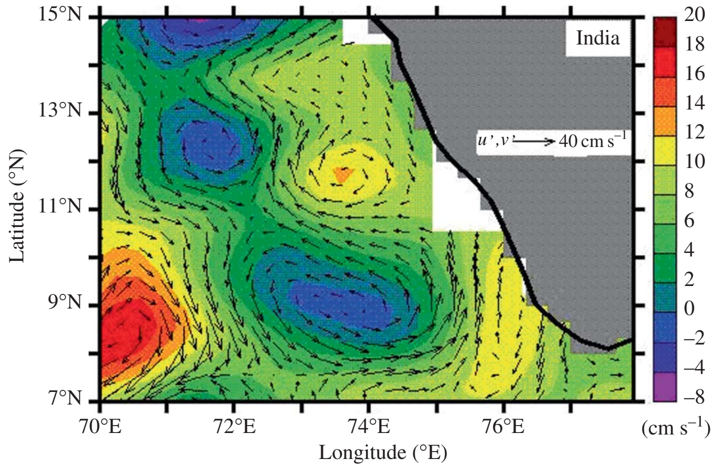

Figure 5. Horizontal distribution of sea surface height anomaly (SSHA) overlaid with geostrophic currents derived from AVISO T/P merged sea level anomalies for 14–18 March 2004.

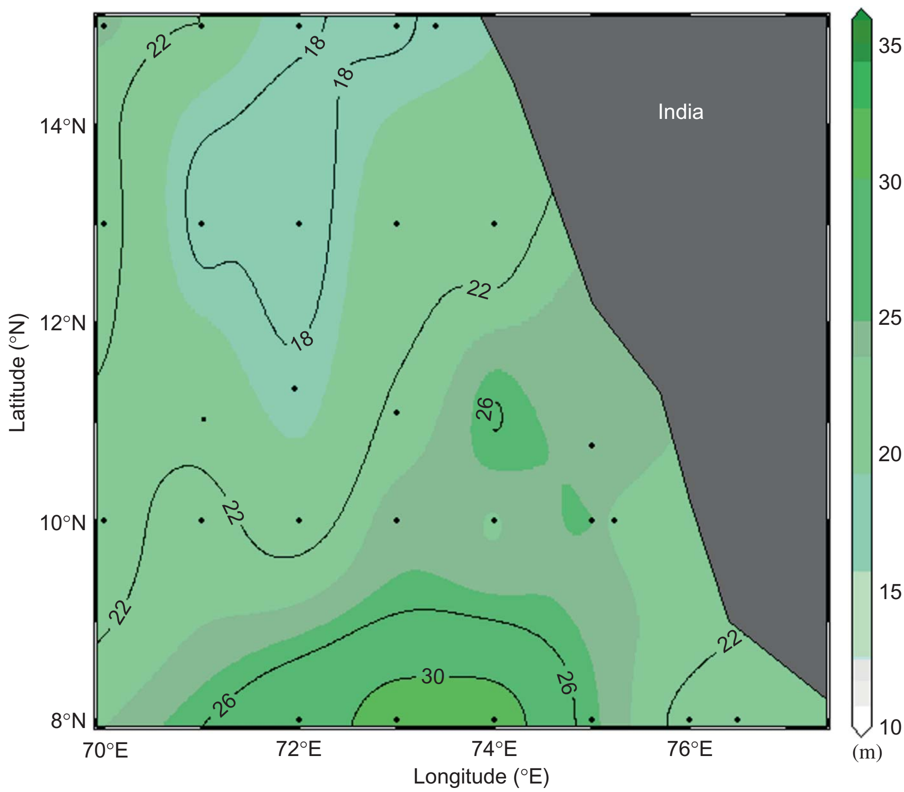

Figure 6. Mixed layer depth (m) of the study region.

4.1 *Temperature tendency*

The temperature tendency is an order of magnitude weaker than other heat budget terms and it represents the net effect of a combination of other mixed layer processes such as advection, vertical mixing, horizontal diffusion and surface heat fluxes. The temperature tendencies of the ASWP are positive (i.e. warming) in the northeastern side of the warm pool with a maximum value approaching 1.5×10^{-6} °C s^{-1} at the coast (figure 7). The warming in the northwest of the study area is due to the inwards net surface flux into the ocean (figure 8). The tendency of the mixed layer temperature shows that the mixed layer warming in the northern part of the warm pool mainly follows the surface heat flux. It indicates that the northern part of the ASWP surface heat flux has a larger control on the mixed layer warming.

In the southeastern part of the warm pool (south of 11° N), the spatial variability of the temperature tendency has a horizontal size of nearly 100 km. Positive and negative temperature tendencies the size of eddies are a prominent feature in this region (figure 7). Here, the temperature tendency does not vary in accordance with the surface heat flux. This is the region where mesoscale features were prominent during the study period as we have identified from the altimetry data. The magnitude of this warming is only 10% of that of the warming in the north (figure 7).

4.2 *Advection*

Advection is the process by which a local gradient of material property (here it is the temperature) is being transported horizontally according to the currents. The advection of the northeastern part of the warm pool shows a strong positive value

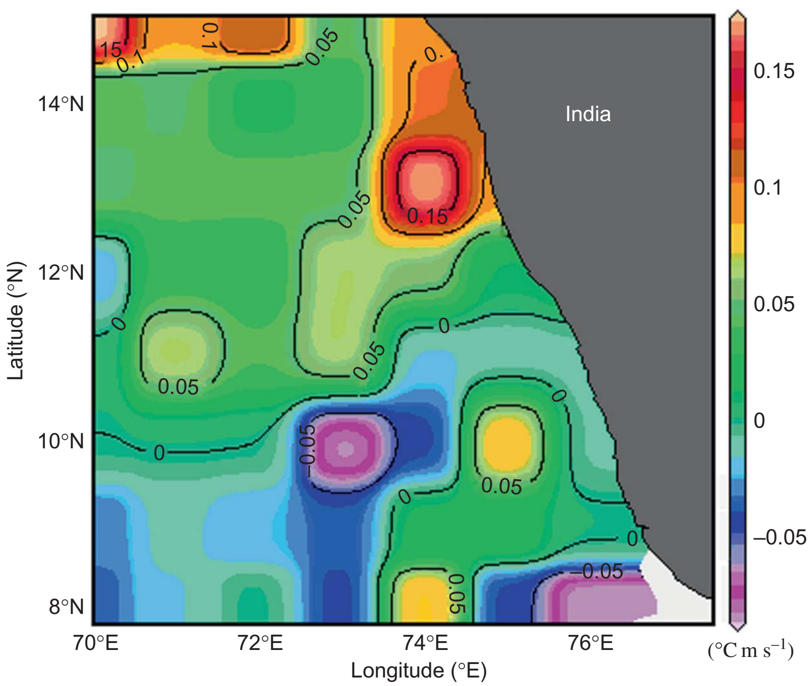

Figure 7. Temperature tendency in the mixed layer ($\times 10^{-5}$) integrated over the entire mixed layer depth. Units are in °C m s^{-1}.

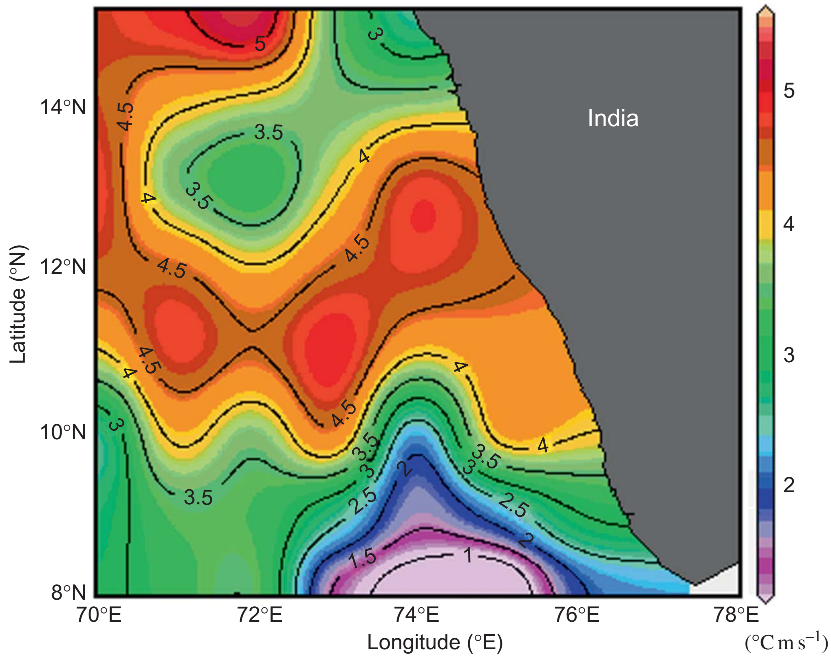

Figure 8. Surface flux ($\times 10^{-5}$) from the observations. Positive values mean heat flux into the ocean. Units are in °C m s^{-1}.

indicating the advective warming (figure 9). The advection patterns in the warm pool area show strong positive contours oriented parallel to the coast up to the central region. The background mixed layer temperature was warmer on the coastal side and relatively colder farther west (figure 3(*a*)). Thus, the effect of advection reduces this gradient by transferring more warm water to the western side of the warm pool and causing an advective warming in the west. The magnitude of advection in the north-western part of the warm pool region is 0.5×10^{-5} °C m s^{-1}, which is only 10% of the net surface heat flux.

In the northern part of the warm pool, the surface heat flux shows the highest value (figure 8). The advection delineates a zero contour running northwest and passing through the centre of the study region (figure 9). To the east of the zero contours, the advection warms the region. Thus, the highest surface heat flux into the ocean in the northern part is exported to the west, further warming the western side of the warm pool. Thus, advection exports the heat from the warm pool, which mostly comes as the surface heat flux in the northern side. This export causes the mixed layer depth to an average value of 25 m in the northwest. In the extreme southeast, the temperature tendency (figure 7) shows a strong cooling as explained by the negative advection.

The effect of local wind and subsequent Ekman transport is computed separately and compared with the geostrophic currents in order to find the impact of Ekman transport on the total advection of heat in the mixed layer. It is found that the Ekman velocity is much smaller than the near surface geostrophic currents. The analysis period represents the transition period of the monsoon (from northeast to southwest monsoon), and thus the winds are, generally, weaker and resulting in a weaker Ekman

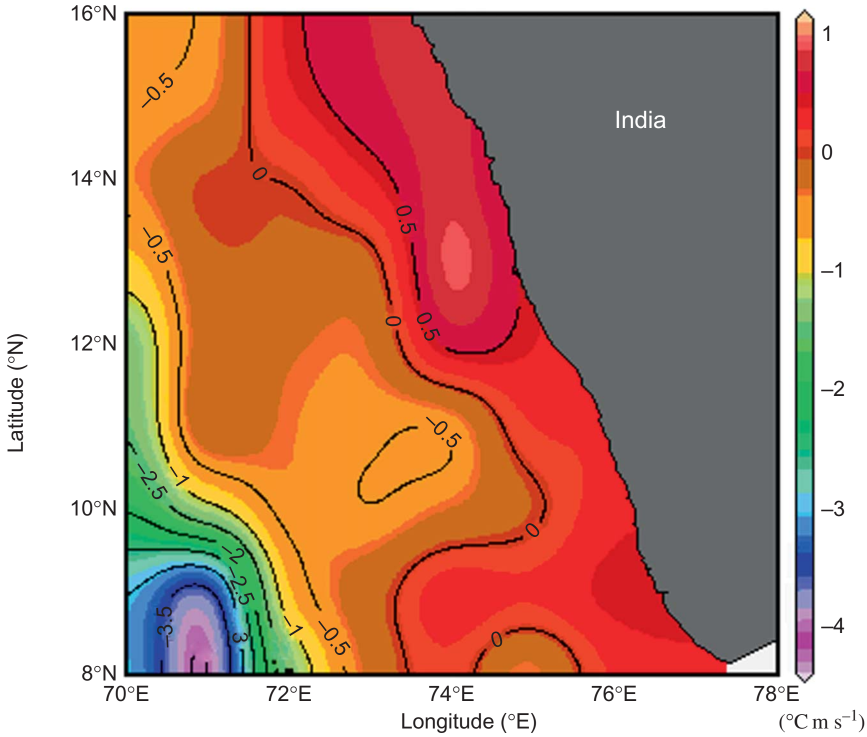

Figure 9. Horizontal advection (geostrophic currents alone) vertically integrated over the mixed layer ($\times 10^{-5}$). Units are in °C m s^{-1}.

drift than the background geostrophy. We have also computed the advection terms with a total current of geostrophy and Ekman drift and found no appreciable differences in the advection term compared to the non Ekman drift case, except small changes in the south (figure 10).

4.3 *Diffusion*

Unlike the advection, the effect of horizontal diffusion is not so significant in the northeastern part of the domain (figure 11). The average value of diffusion is nearly zero in the northeastern part of the domain where advection showed a warming effect. The effect of eddy diffusion becomes significant on the southern part of the domain where eddy features were prominent. The maximum diffusion in the southern part of the domain is found to be 2.5×10^{-5} °C m s^{-1}, which is greater than the amount of advection there (figure 8). The effect of eddy induced diffusion is to smooth the temperature gradient. Over the southern part of the domain, the eddy induced diffusion has mesoscale features and smoothes the temperature gradient there. It is interesting to note that the mixed layer temperature tendency also follows the diffusion term in its spatial scale. Thus, the effect of eddy induced smoothing of temperature in the mixed layer is prominent in the southern part of the warm pool region. The surface heat flux does not have such fine scale structures to reflect in the temperature tendency as evident from figure 6.

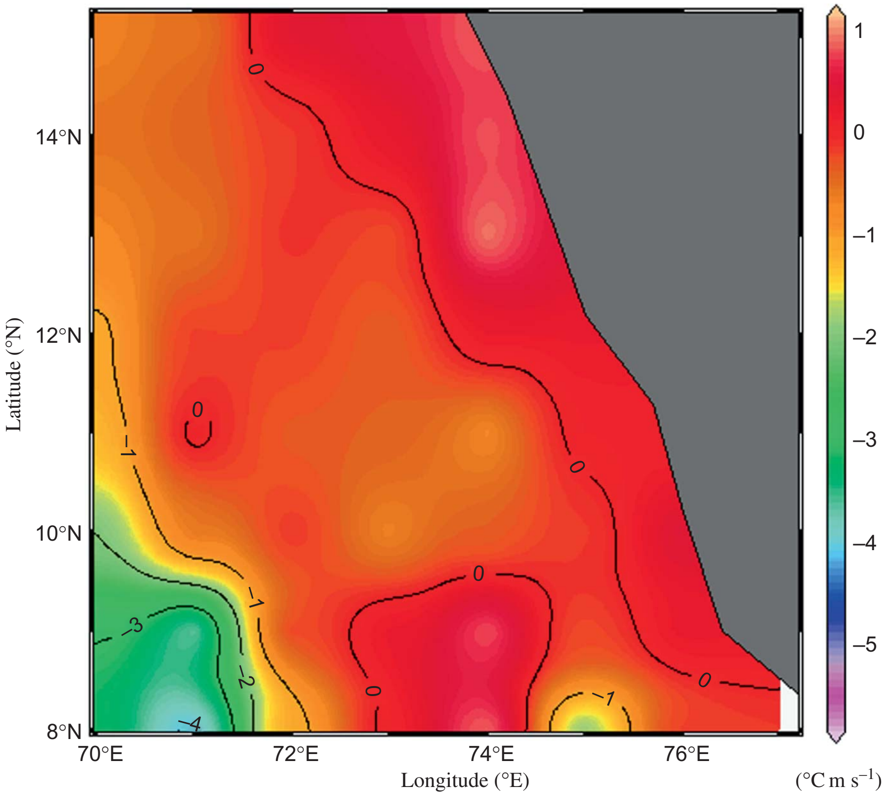

Figure 10. Horizontal advection (geostrophic + Ekman currents) vertically integrated over the mixed layer ($\times 10^{-5}$). Units are in °C m s^{-1}.

The magnitude of diffusion in the southern part of the warm pool region suggests an eddy diffusion coefficient to be as large as $A_h = 3 \times 10^4$ m^2 s^{-1}. This high value resolved in our analysis is of course partially related to the coarse resolution of the data (1° × 1° spatial grid). The presumtion of a high eddy diffusion coefficient, shown by the data analysis, implies that a coarse resolution model should include this large value of eddy diffusion coefficient, in order to have a reasonable account of eddy induced lateral mixing. However, such a large value of eddy diffusion smoothes out the mesoscale variability in a numerical model. This eventually points to the necessity of resolving eddy induced diffusion as an indirect estimate of eddy induced transport as in the widely used Gent and McWilliams parameterization (Gent and McWilliams 1990). Our analysis shows that for the models to have a reasonable simulation of diffusive processes in the ASWP, especially in the southern part of the domain, either finer resolution data are necessary to resolve mesoscale induced mixing reasonably or an indirect parameterization of eddy induced transports should be included.

4.4 *Vertical mixing*

Although the horizontal advection, diffusion and surface heat fluxes can account for the major features of the temperature tendency qualitatively, the effect of vertical mixing should also be considered for the detailed account of surface heat budget.

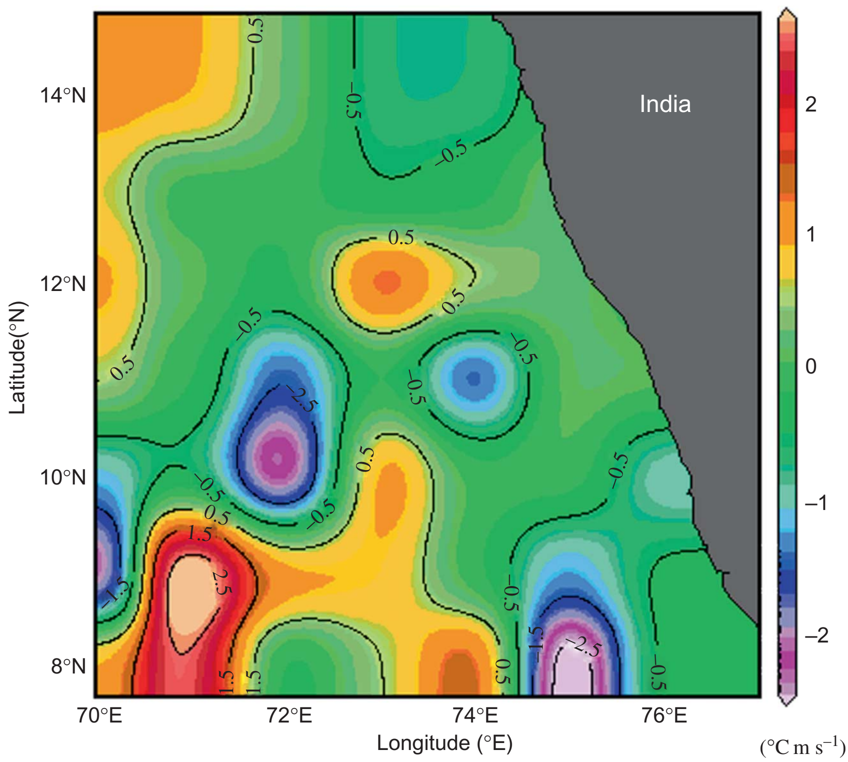

Figure 11. Diffusion term ($\times 10^{-5}$) vertically integrated over the mixed layer. Units are in °C m s^{-1}.

Figure 12 shows the vertical mixing term integrated over the mixed layer. The negative values show the cooling by deepening of the mixed layer and positive values show the warming by shoaling of the mixed layer. Unlike the other terms presented above, the vertical mixing did not exhibit any similarity with the temperature tendency except in the southern domain. In the southern part of the domain, the vertical mixing features of size of the order of 100 km in the horizontal, similar to the eddy induced heat flux and temperature tendency. The magnitude of the vertical mixing is stronger in the south due to the strong eddy induced current in the region.

The study area is divided into two boxes (*a*) north box (B_N) (area between 12° N and 15° N) and (*b*) south box (B_S) (area between 8° N and 11° N). The vertically integrated mixed layer heat budget terms were spatially averaged for each box (figure 13). The surface heat flux is stronger in the north than in the south. The vertical mixing dominates the advection in the southern part. This is clearly evident in the deeper mixed layer depth as seen in the southern part of the SEAS (figure 6). The input surface heat is thus balanced between vertical mixing and horizontal advection in the southern part of the domain. The eddy diffusion shows a slight warming although the magnitude is relatively lower than the advection or vertical mixing. In the northern part (B_N), the surface heat flux is balanced between advection and diffusion while in the southern domain (B_S), the advection dominates over vertical mixing and the horizontal diffusion is negligible.

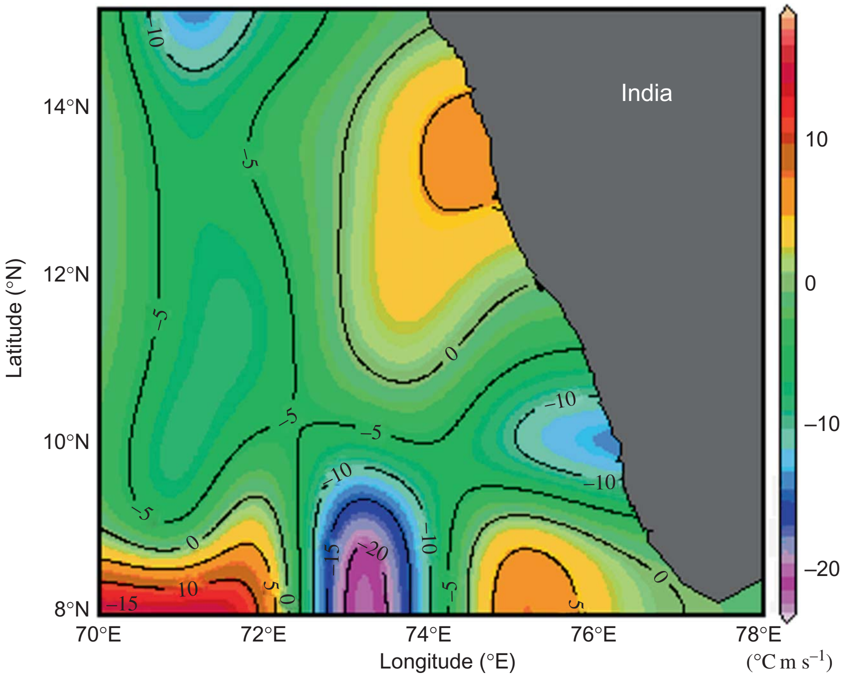

Figure 12. Mixing term ($\times 10^{-5}$) vertically integrated over the mixed layer. Units are in $°C\ m\ s^{-1}$.

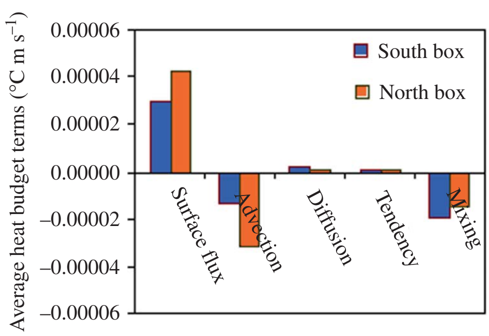

Figure 13. The average heat budget over the north and south of the study region. Units are in $°C\ m\ s^{-1}$.

5. Conclusion

The importance of various mixed layer processes (advection, eddy induced diffusion, vertical mixing and surface flux) on the formation of ASWP during the spring inter-monsoon were discussed. The study shows that a considerable spatial variation exists in the mixed layer processes of the ASWP. The surface heat flux was the dominant component in the mixed layer warming in the northern part of the ASWP, whereas advection has only a subsidiary role in spreading the warm pool from the coast to offshore. In the south of the domain, the effect of eddy induced transport is seen to be as important as the advection. This is mainly associated with the prominence of the eddy in that region during the transition of monsoon.

The study is not a climatological representation of the warmpool mixed layer processes because of the limited data. The coarse resolution of the data limited our chance to get a closer look into the more detailed processes of the mixed layer heat budget evolution of ASWP. With the available *in situ* data, our study categorized the significance of various mixed layer processes and its regional dominance throughout the evolution of ASWP. The study also dictates those processes that are necessary for a reasonable simulation of the regional modelling of the ASWP.

Acknowledgements
We thank Dr S.R. Shetye, Director, National Institute of Oceanography, Goa, and Dr V.N. Sanjeevan, Director, Centre for Marine Living Recourses and Ecology, Kochi, for providing facilities for the study. We are also thankful to all the participants of Cruise No. 223 of FORV Sagar Sampada for the help with sampling. We are grateful to Dr Vinu Valsala, National Institute of Environmental Studies, Tsukuba, Ibaraki, Japan, for his help, guidance and valuable suggestions. The first author acknowledges the financial support from CSIR. This investigation was carried out under the MR-LR programme funded by the Ministry of Earth Sciences, Government of India, New Delhi. This is NIO contribution No. 4780.

References

ANONYMOUS, 2001, Arabian Sea monsoon experiment (ARMEX): Science plan. Department of Science and Technology, Government of India, New Delhi. Available online at: http://caos.iisc.ernet.in/hpg/armscience.html (accessed April 2004).

BRUCE, J.G., JOHNSON, D.R. and KINDLE, J.C., 1994, Evidence for eddy formation in the eastern Arabian Sea during the northeast monsoon. *Journal of Geophysical Research*, **99**, pp. 7651–7664.

CURRY, J.A. and WEBSTER, P.J., 1998, Thermodynamics of atmospheres and oceans. *International Geophysics Series*, **65**, pp. 1–456.

CUTLER, A.N. and SWALLOW, J.C., 1984, Surface currents of the Indian Ocean (to 25°S, 100°E): compiled from historical data archived by the Meteorological Office. Institute of Oceanographic Sciences Report No. 187, Bracknell, UK, p. 42.

DURAND, F., SHETYE, S.R., VIALARD, J., SHANKAR, D., SHENOI, S.S.C., ETHE, C. and MADEC, G., 2004, Impact of temperature inversions on SST evolution in the south-eastern Arabian Sea during the pre-summer monsoon season. *Geophysical Research Letters*, **31**, L01305, doi: 10.1029/2003GL018906.

GENT, P.R. and MCWILLIAMS, J.C., 1990, Isopyncal mixing in ocean circulation models. *Journal of Physical Oceanography*, **20**, pp. 150–155.

GOPALAKRISHNA, V.V., JOHNSON, Z., SALGAONKAR, G., NISHA, K., RAJAN, C.K. and RAO, R.R., 2005, Observed variability of sea surface salinity and thermal inversions in the Lakshadweep Sea during contrast monsoons. *Geophysical Research Letters*, **32**, L18605, doi: 10.1029/2005GL023280.

GROTZNER, A., LATIF, M. and BARNETT, T.P., 1998, A decadal climate cycle in the North Atlantic Ocean as simulated by the ECHO coupled GCM. *Journal of Climate*, **11**, pp. 831–847.

JOHANNESSEN, O.M., SUBBARAJU, G. and BLINEDHEIM, J., 1987, Seasonal variations of the oceanographic conditions off the southwest coast of India during 1971–1975. *Fiskeridirektoratet Skrifter Serie Havundersoekelser*, **18**, pp. 247–261.

JOSEPH, P.V., 1990, Warm pool over the Indian Ocean and monsoon onset. *Tropical Ocean Atmosphere News Letter*, **53**, pp. 1–5.

Josey, S.A., Kent, E.C. and Taylor, P.K., 1999, New insights into the ocean heat budget closure problem from analysis of the SOC air–sea flux climatology. *Journal of Climate*, **12**, pp. 2856–2880.

Kurian, J. and Vinayachandran, P.N., 2006, Formation mechanisms of temperature inversions in the southeastern Arabian Sea. *Geophysical Research Letters*, **33**, L17611, doi: 10.1029/2006GL027280.

Kurian, J. and Vinayachandran, P.N., 2007, Mechanisms of formation of the Arabian Sea mini warm pool in a high-resolution ocean general circulation model. *Journal of Geophysical Research*, **112**, C05009, doi: 10.129/2006JC003631.

Large, W.G., Williams, J.C. and Doney, S.C., 1994, Oceanic vertical mixing: a review and a model with a nonlocal boundary layer parameterization. *Reviews of Geophysics*, **32**, pp. 363–403.

Liu, Q., Xie, S.-P., Li, L. and Maximenko, N.A., 2005, Ocean thermal advective effect on the annual range of sea surface temperature. *Geophysical Research Letters*, **32**, L24604, doi: 10.1029/2005GL024493.

Lukas, R., 1988, On the role of western Pacific air–sea interaction in the El Niño/Southern Oscillation phenomenon. In *Proceedings of the US TOGA Western Pacific Air–Sea Interaction Workshop*, 16–18 September 1987, Honolulu, US TOGA Report USTOGA-8, R. Lukas and P. Webster (Eds) (Boulder, CO: University Corporation for Atmospheric Research), pp. 43–69.

Lukas, R. and Lindstrom, E., 1991, The mixed layer of the western equatorial Pacific Ocean. *Journal of Geophysical Research*, **96** (Supplement), pp. 3343–3358.

Madhupratap, M., Gauns, M., Ramaiah, N., PrasannaKumar, S., Muraleedharan, P.M., deSousa, S.N., Sardessai, S. and Muraleedharan, U.D., 2003, Biogeochemistry of the Bay of Bengal: physical, chemical and primary productivity characteristics of the central and western Bay of Bengal during summer monsoon 2001. *Deep-Sea Research II*, **50**, pp. 881–896.

Masson, S., Delecluse, P. Boulanger, J.P. and Menkes, C., 2002, A model study of the seasonal variability and formation mechanisms of the barrier layer in the eastern equatorial Indian Ocean. *Journal of Geophysical Research*, **107**, 8017, doi: 10.1029/2001JC000832.

Murty, V.S.N., Krishna, S.M., Nagaraju, A., Somayajulu, Y.K., Remeshbabu, V., Sengupta, D., Sindu, P.R., Ravichandran, M. and Rajesh, G., 2006, On the warm pool dynamics in the southeastern Arabian Sea during April–May 2005 based on the satellite remote sensing and ARGO float data. *Proceedings of SPIE*, **6406**, doi: 10.1117/12.694254.

Pond, S. and Pickard, G.L. (Eds), 1983, *Introduction to Dynamic Oceanography* (2nd edn) (Woburn, MA: Butterworth-Heinemann).

Prasad, T.G. and Ikeda, M., 2002, The winter-time water mass formation in the northern Arabian Sea: a model study. *Journal of Physical Oceanography*, **32**, pp. 1028–1040.

PrasannaKumar, S. and Prasad, T.G., 1996, Winter cooling in the northern Arabian Sea. *Current Science*, **71**, pp. 834–841.

Qiu, B., 2002, The kuroshio extension system. Its large-scale variability and role in the midlatitude ocean–atmosphere interaction. *Journal of Oceanography*, **58**, pp. 57–75.

Qiu, B. and Chen, S., 2004, Eddy-induced heat transport in the subtropical North Pacific from Argo, TMI and altimetry measurements. *Journal of Physical Oceanography*, **35**, pp. 458–473.

Rao, R.R. and Sivakumar, R., 1999, On the possible mechanisms of the evolution of a mini-warm pool during the pre-summer monsoon season and the onset vortex in the southeastern Arabian Sea. *Quarterly Journal of the Royal Meteorological Society*, **125**, pp. 787–809.

Shankar, D., Gopalakrishna, V.V., Shenoi, S.S.C., Durand, F., Shetye, S.R., Rajan, C.K., Johnson, Z., Araligidad, N. and Michael, G.S., 2004, Observational evidence for westward propagation of temperature inversions in the southeastern Arabian Sea. *Geophysical Research Letters*, **31**, L08305, doi: 10.1029/2004GL019652.

SHANKAR, D. and SHETYE, S.R., 1997, On the dynamics of the Lakshadweep high and low in the southeastern Arabian Sea. *Journal of Geophysical Research*, **102**, pp. 12 551–12 562.

SHENOI, S.S.C., SHANKAR, D. and SHETYE, S.R., 1999, On the sea surface temperature high in the Lakshadweep Sea before the onset of the southwest of monsoon. *Journal of Geophysical Research*, **104**, pp. 15 703–15 712.

SHENOI, S.S.C., SHANKAR, D. and SHETYE, S.R., 2004, Remote forcing annihilates barrier layer in southeastern Arabian Sea. *Geophysical Research Letters*, **37**, L05307, doi: 10.1029/2003GL019270.

SHETYE, S.R., GOUVEIA, A.D., SHANKAR, D., SHENOI, S.S.C., VINAYACHANDRAN, P., SUNDAR, N., MICHAEL, G.S. and NAMBOODIRI, G., 1996, Hydrography and circulation in the western Bay of Bengal during the northeast monsoon. *Journal of Geophysical Research*, **101**, pp. 14 011–14 025.

SHETYE, S.R., GOUVEIA, A.D., SHENOI, S.S.C., MICHAEL, G.S., SUNDAR, D., ALMEIDA, A.M. and SANTANAM, K., 1991, The coastal current off western India during the northeast monsoon. *Deep Sea Research, Part A*, **38**, pp. 1517–1529.

SMYTH, W.D., HEBERT, D. and MOUM, J.N., 1996, Local ocean response to a multiphase westerly wind burst: 2. Thermal and freshwater responses. *Journal of Geophysical Research*, **101**, pp. 22 513–22 534.

STEWART, R.H., 2007, Introduction to physical oceanography. Texas A & M University. Available online at: http://www.ocean.ukm.my/physicaloceanographysteaward.pdf (accessed 27 March 2009).

THADATHIL, P. and GOSH, A.K., 1992, Surface layer temperature inversion in the Arabian Sea during winter. *Journal of Oceanography*, **48**, pp. 293–304.

VINAYACHANDRAN, P.N. and SHETYE, S.R., 1991, The warm pool in the Indian Ocean. *Proceedings of the Indian Academy of Sciences (Earth Planetary Sciences)*, **100**, pp. 165–175.

WANG, C. and WEISBERG, R.H., 2001, Ocean circulation influences on sea surface temperature in the equatorial central Pacific. *Journal of Geophysical Research*, **106**, pp. 19 515–19 526.

WEBSTER, P.J., PALMER, T.N., MAGANA, V.O., SHUKLA, J., TOMAS, R.A., YANAI, T.M. and YASUNARI, A., 1998, Monsoons: processes, predictability and the prospects for prediction. *Journal of Geophysical Research*, **103**, pp. 14 451–14 510.

WELLER, R.A., FISCHER, A.S., RUDNICK, D.L., ERIKSON, C.C., DICKEY, T.D., MARRA, J., FOX, C. and LEBEN, R., 2002, Moored observations of upper ocean response to the monsoon in the Arabian Sea during 1994–1995. *Deep Sea Research-II*, **49**, pp. 2195–2230.

WIGGERT, J.D., HOOD, R.R., BANSE, K. and KINDLE, J.C., 2005, Monsoon-driven biogeochemical processes in the Arabian Sea. *Progress in Oceanography*, **65**, pp. 176–213.